


Article

Experimental Study on Simultaneous Desulfurization and Denitrification by DBD Combined with Wet Scrubbing

Liang Yang¹, Yunkai Cai^{2,*}  and Lin Lu²¹ Guangxi Yuchai Machinery Co, Ltd., Yulin 537005, China; 15977502759@163.com² School of Energy and Power Engineering, Wuhan University of Technology, Wuhan 430070, China; lulinwhut@whut.edu.cn

* Correspondence: caiyunkai@whut.edu.cn; Tel.: +86-1562-372-3935

Abstract: A dielectric barrier discharge (DBD) reactor combined with a wet scrubbing tower was used to carry out an experimental study on desulfurization and denitrification. The effects of the packing type, packing height, spray density, mass fraction of the NaOH solution, discharge power in the DBD reactor, and simulated flue gas flow rate on the desulfurization and denitrification efficiency were analyzed, along with the influence weight of each factor, using orthogonal testing. The experimental results showed that SO₂ was easily absorbed by the scrubbing solution, while the desulfurization efficiency remained at a high level (97–100%) during the experiment. The denitration efficiency was between 12 and 96% under various operating conditions. Denitration is the key problem in this system. The influence weights of the DBD power, simulated flue gas flow rate, mass fraction of the NaOH solution, spray density, packing type, and packing height on the denitration efficiency were 56.96%, 18.02%, 11.52%, 5.02%, 4.33%, and 4.16%, respectively. This paper can provide guidance to optimize the desulfurization and denitrification efficiency of this DBD reactor combined with a wet scrubbing system.



Citation: Yang, L.; Cai, Y.; Lu, L. Experimental Study on Simultaneous Desulfurization and Denitrification by DBD Combined with Wet Scrubbing. *Appl. Sci.* **2021**, *11*, 8592. <https://doi.org/10.3390/app11188592>

Academic Editor: Hyun-Seog Roh

Received: 23 August 2021

Accepted: 14 September 2021

Published: 16 September 2021

Publisher's Note: MDPI stays neutral with regard to jurisdictional claims in published maps and institutional affiliations.



Copyright: © 2021 by the authors. Licensee MDPI, Basel, Switzerland. This article is an open access article distributed under the terms and conditions of the Creative Commons Attribution (CC BY) license (<https://creativecommons.org/licenses/by/4.0/>).

Keywords: DBD; wet scrubbing; desulfurization; denitrification

1. Introduction

Ocean-going ships undertake more than 90% of the global cargo transportation tasks; however, the pollutants in their exhaust emissions (such as NO_x and SO_x) also cause serious air pollution and endanger human health [1,2]. NO_x and SO_x are important components in the formation of photochemical smog in the atmosphere, the destruction of the atmospheric ozone layer, and acid rain. In order to control exhaust emissions from ships, the International Maritime Organization (IMO) revised Annex VI of MARPOL 73/78 convention to limit NO_x and SO_x emissions, as shown in Figure 1 [3]. Due to increasingly stringent regulations, it is imperative to develop highly efficient desulfurization and denitration technologies for ships.

Selective catalyst reduction (SCR) is the main method used to remove NO_x, the denitration efficiency of which can reach more than 90%; however, SO₂ in ship exhausts will cause sulfur poisoning of the SCR catalyst and reduce the catalyst's efficiency [4,5]. The effective way to avoid sulfur poisoning is to place the SCR system behind the wet desulfurization unit, although the SCR system will face the problem of low exhaust temperature.

Due to the high efficiency and technical maturity of the wet scrubbing gas desulfurization (WFGD) system, it has been widely applied for ship desulfurization [3,6]. Wet-type desulfurization and denitration technologies are easy to integrate with WFGD, reducing the investment cost and floor space of the whole system; therefore, on the basis of ship WFGD, wet-type desulfurization and denitration technologies will be important development directions for ship exhaust gas treatment technology in the future [7].

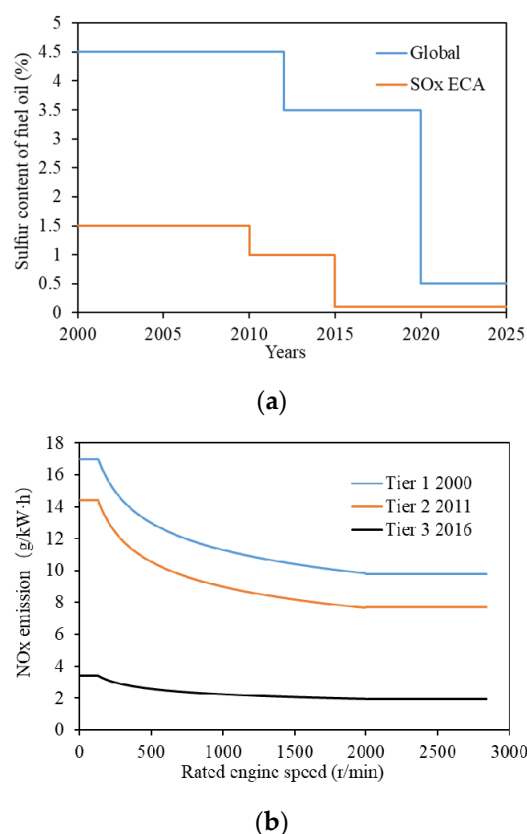


Figure 1. IMO emission regulation limits: (a) SO_x emission limits; (b) NO_x emission limits.

The denitration efficiency of the WFGD system is insufficient [8]. This is because more than 95% of NO_x in the exhaust exists in the form of NO, which is difficult to dissolve in water. The oxidation of NO to NO₂ is an effective way to improve the denitration efficiency of the wet scrubbing system. At present, the methods used for NO oxidation mainly include the use of oxidants (such as KMnO₄ [9], ClO₂ [10], O₃ [11–14], H₂O₂ [15,16], NaClO₂ [17,18]), seawater electrolysis technology [19], and non-thermal plasma (NTP) technology [20]. Among them, NTP technology has the advantages of low investment and operation costs, and has become a research hotspot in terms of flue gas treatment [21,22].

Yu et al. built a DBD reactor combined with a seawater scrubbing system for a diesel engine, achieving removal efficiencies for NO_x and SO₂ of 70% and 90%, respectively [23]. Xie et al. investigated the effects of different scrubbing solutions (Na₂SO₃, FeSO₄, Na₂SO₄) on the denitration efficiency using NTP oxidation combined with wet scrubbing [24]. Zhang et al. established a one-dimensional model for a plasma chemical reaction process involving desulfurization and denitration via corona discharge [25]. Chmielewski et al. built an electron beam (EB) combined with a seawater scrubbing system, and the effects of the EB dose and NO and SO₂ concentrations on desulfurization and denitration were investigated [26]. Gui et al. proposed a DBD reactor combined with a wet electrostatic precipitator (WESP) system and studied the effects of the specific energy density (SED) and NO and SO₂ concentrations [27]. Zwoli et al. used an EB combined with a wet scrubber for desulfurization and denitration, and the effects of the pollutant concentration, scrubbing solutions (NaCl, NaOH, H₂O₂, NaClO₂), and gas flow rate were investigated [28]. Zhao et al. studied the effects of NaClO, NaClO₂, and NaClO₃ solutions on denitration using an EB combined with a wet scrubber [29]. In our previously studies, we discussed the effects of the DBD reactor structure on the oxidative removal of NO and SO₂ [30,31].

There are many factors affecting the desulfurization and denitration efficiency of NTP combined wet scrubbing; however, studies have rarely analyzed the effects of the system structure and the influence weight of each factor. Additionally, it is difficult to

achieve system optimization. In this paper, an experimental study on desulfurization and denitration is carried out using a DBD reactor combined with a wet packed scrubber. The effects of the packing type, packing height, spray density, mass fraction of the NaOH solution, discharge power in the DBD reactor, and simulated flue gas flow rate on the desulfurization and denitration efficiency are analyzed, along with the influence weight of each factor, using orthogonal testing.

2. Experiment and Methods

2.1. Experiment Setup

The schematic diagram of the experimental setup is presented in Figure 2. It consists of a gas feeding system, an NTP oxidation system, a discharge power measurement system, a wet scrubbing system, and a fuel gas analyzer.

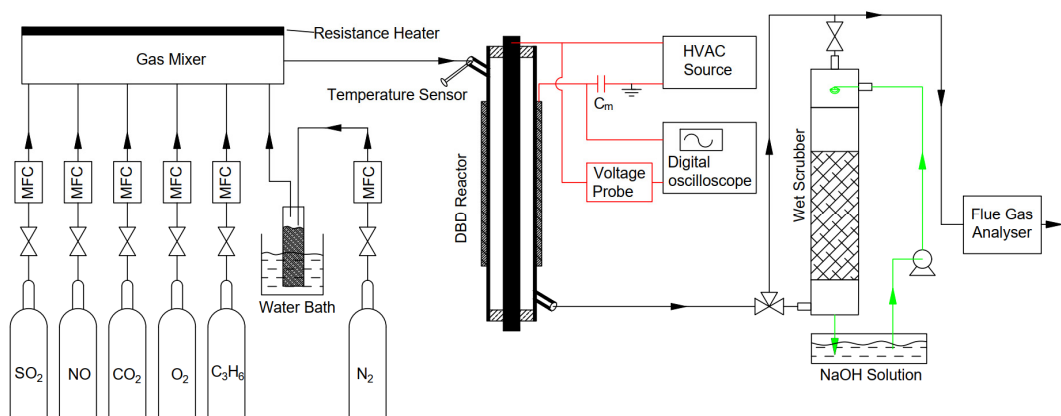


Figure 2. The schematic diagram of the experimental setup.

In this setup, the marine diesel exhaust was simulated using a gas mixture of 10% O₂, 7% CO₂, 6.6% H₂O, 200 ppm C₃H₆, 820 ppm NO, 320 ppm SO₂, and N₂ (balance). The simulated flue gas temperature at the DBD reactor inlet was 115 °C.

The NTP oxidation system consisted of a coaxial cylindrical DBD reactor and an AC high-voltage power supply. A stainless steel rod with a diameter of 14 mm was used as the inner electrode of DBD reactor. A quartz tube with an outer diameter of 18 mm, an inner diameter of 15 mm, and a length of 450 mm was used as the dielectric layer. The quartz tube was wrapped with copper foil as the outer electrode with a length of 100 mm. The CTP-2000K system (Nanjing is plasma Co., Ltd., Nanjing, China) was used as a power supply for the NTP. The discharge frequency was fixed at 10 kHz and the discharge power in DBD reactor was controlled by adjusting discharge voltage.

The packed scrubber was placed after the DBD reactor with an inner diameter of 25 mm and a height of 150 cm. The packing equipment used in the experiment included Cannon rings, Pall rings, and Dixon rings, as shown in Figure 3. The concentrations of NO, NO₂, O₂, CO₂, and SO₂ were measured using a flue gas analyzer (TESTO Pro.350), with the information from TESTO Pro.350 shown in Table 1.



(a)



(b)



(c)

Figure 3. The packing equipment used in the experiment. (a) Cannon rings; (b) Pall rings; (c) Dixon rings.

Table 1. The information obtained from TESTO Pro.350.

Sensor	Range	Accuracy	Resolution	Response Time
NO	0–2000 ppm	5 ppm (0–99 ppm) ±5% of the measured value (100–2000 ppm)	1 ppm	30 s
NO ₂	0–500 ppm	5 ppm (0–99 ppm) ±5% of the measured value (100–2000 ppm)	0.1 ppm	40 s
SO ₂	0–2000 ppm	±5% of the measured value	1 ppm	30 s
O ₂	0–25 Vol%	±0.2 Vol%	0.01%	20 s
CO ₂	0–25 Vol%	±0.3 Vol% + 1% of the measured value	0.01%	20 s

2.2. Data Processing

The discharge voltage and current waveforms are shown in Figure 4a. There were many micro discharge channels in the gas gap of the DBD reactor. It is difficult to measure the discharge power using the integral of voltage and current product; therefore, the discharge power in DBD reactors is usually measured using the Q-V Lissajous figure, which requires a capacitor (C_m) in series in the DBD circuit. Figure 4b shows the Lissajous figure measured during the experiment. The discharge power is calculated by:

$$P = fC_mK_xK_yKA \quad (1)$$

where f is the discharge frequency in Hz; K_x is the X-axis sensitivity, V/grid; K_y is the Y-axis sensitivity, V/grid; K is the voltage decrease ratio, 1000:1; A is the area enclosed by the Lissajous figure.

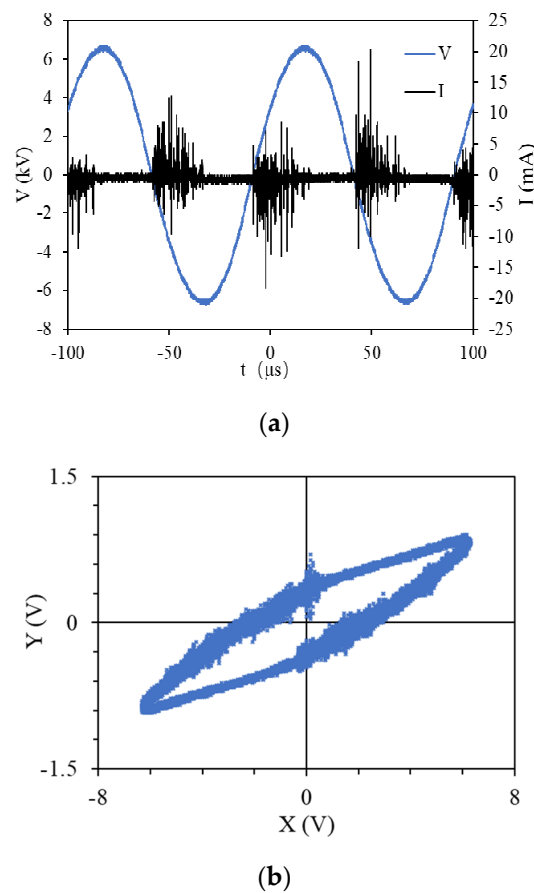


Figure 4. The current and voltage waveforms for the DBD reactor: (a) the voltage and current waveforms; (b) the Lissajous figure.

The removal efficiency of NO_x is calculated using the following formula:

$$\text{Removal efficiency of } \text{NO}_x = \frac{[\text{NO}_x]_{\text{inlet}} - [\text{NO}_x]_{\text{outlet}}}{[\text{NO}_x]_{\text{inlet}}} \times 100\% \quad (2)$$

where $[\text{NO}_x]_{\text{inlet}}$ and $[\text{NO}_x]_{\text{outlet}}$ are the concentrations of NO_x (ppm) measured at the inlet and outlet of the DBD reactor, respectively.

The removal efficiency of SO_2 is calculated using the following formula:

$$\text{Removal efficiency of } \text{SO}_2 = \frac{[\text{SO}_2]_{\text{inlet}} - [\text{SO}_2]_{\text{outlet}}}{[\text{SO}_2]_{\text{inlet}}} \times 100\% \quad (3)$$

where $[SO_2]_{inlet}$ and $[SO_2]_{outlet}$ are the concentrations of SO_2 (ppm) at the inlet and outlet of the DBD reactor, respectively.

The oxidation degree of NO_x is defined as follows:

$$\alpha_0 = \frac{\varphi(NO_2)}{\varphi(NO_x)} \times 100\% \quad (4)$$

where α_0 is the oxidation degree of NO_x ; $\varphi(NO_2)$ is the concentration of NO_2 in ppm; $\varphi(NO_x)$ is the concentration of NO_x ($NO + NO_2$) in ppm.

3. Results and Discussion

3.1. The Packing Types

The packing is the core component of the packed scrubber, the configuration of which is directly related to the gas–liquid mass transfer efficiency. The surface of packing is the basis of gas–liquid mass transfer in the scrubbing tower [32]. During the experiment, the simulated fuel gas was preoxidized by the DBD reactor and the discharge power was fixed at 19.5 W. The effects of different packing on desulfurization and denitration efficiency were investigated and the results are shown in Figure 5. The experimental results show that the denitration efficiencies of the D_g 10 mm Pall ring, D_g 6 mm Pall ring, D_g 6 mm Dixon ring, and D_g 6 mm Cannon ring are 62.6%, 66.6%, 70.8%, and 65.6%, respectively, while the desulfurization efficiencies are more than 99.3% for all packings.

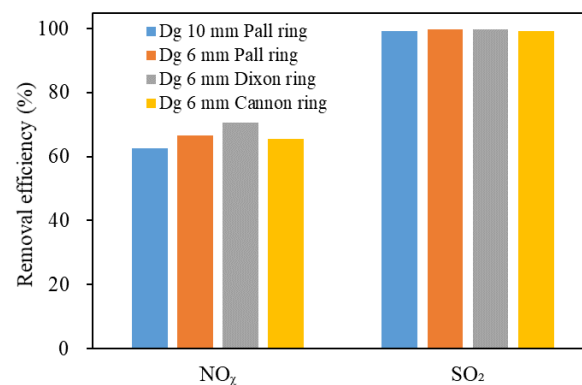


Figure 5. Desulfurization and denitration efficiencies of various packing types (operating conditions: gas flow rate = 5 L/min, scrubbing solution = 1% NaOH solution, spray density = $7.6 \text{ m}^3 / (\text{m}^2 \cdot \text{h})$, packing height = 80 cm).

The main absorption process for the packed scrubber occurs in the part filled with packing. For the micro tower height dh , the mass of the solute transferred between gas and liquid phases in this section per unit time can be calculated using the following formula [32]:

$$X = N_A a S dh \quad (5)$$

where X is the mass of solute transferred between gas and liquid phases in the micro tower section per unit time in kmol/s; N_A is the gas–liquid mass transfer rate in kmol/(s · m²); a is the gas–liquid mass transfer area per unit volume in m²/m³; S is the cross-sectional area of the scrubber in m².

The packings with a larger specific surface area can provide a larger gas–liquid mass transfer area (a) and achieve a greater X . The specific surface areas of the four types of packings used in the experiment are shown in Table 2. Due to the larger specific surface area of the D_g 6 mm Dixon ring, it obtains a higher gas–liquid mass transfer efficiency and denitration efficiency. SO_2 is easily absorbed by aqueous solution, while its removal efficiency depends more on the SO_2 absorption capacity of the scrubbing solution; therefore, the packing types have little effect on the desulfurization efficiency.

Table 2. Packing parameters.

Type	Diameter (mm) × Height (mm)	Specific Surface Area (m ² /m ³)
D _g 10 mm Pall ring	10 × 10	482
D _g 6 mm Pall ring	6 × 6	905
D _g 6 mm Dixon ring	6 × 6	950
D _g 6 mm Cannon ring	6 × 6	910

3.2. Packing Height

The height of the packings determines gas–liquid mass transfer area and residence time of fuel gas in the packings, which has an important effect on the removal of pollutants. Figure 6 shows the desulfurization and denitration efficiency of the system at various packing heights. As the packing height increases from 40 cm to 80 cm, the denitration efficiency increases rapidly from 58.4% to 70.8% and the desulfurization efficiency increases from 99.1% to 100%. When the packing height is in the range of 80–120 cm, the denitration efficiency gradually increases from 70.8% to 71.8%.

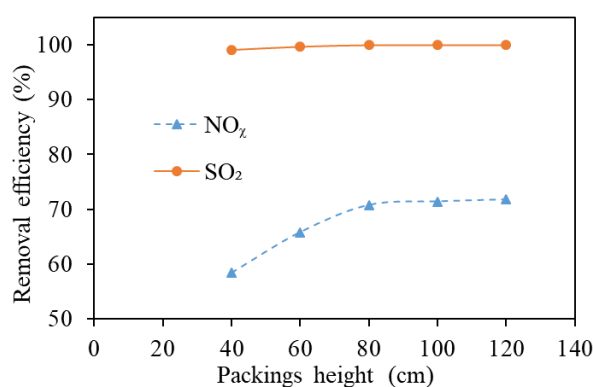


Figure 6. Effect of packing height on desulfurization and denitration efficiency of scrubber (operating conditions: discharge power = 19.5 W; gas flow rate = 5 L/min, scrubbing solution = 1% NaOH solution, spray density = 7.6 m³/(m²·h), packing type = D_g 6 mm Dixon ring).

With the increases in packing height, the gas–liquid mass transfer area and mass transfer time are extended. The desulfurization and denitration efficiency increases with the increase in packing height. For NO_x removal, when the filler height exceeds 80 cm, the remaining NO_x is mainly NO; however, NO has low solubility in water and does not react with NaOH; therefore, the denitration efficiency increases slowly with the increases in packing height in the range of 80–120 cm.

3.3. Spray Density

The spray density is composed of the scrubbing solution spray per unit time and unit tower cross-sectional area, which affects the wetting degree of packings. The effects of the spray density on the desulfurization and denitration efficiency levels are shown in Figure 7. The experimental results show that when the spray density increases from 1.8 m³/(m²·h) to 7.6 m³/(m²·h), the desulfurization efficiency of the system increases from 99.1% to 100% and the denitration efficiency increases from 64.8% to 70.8%. In the range of 7.6–10.8 m³/(m²·h), the desulfurization and denitration efficiency levels remain basically unchanged.

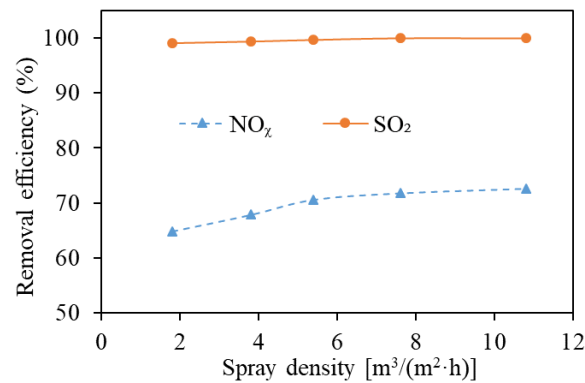


Figure 7. Effects of spray density on desulfurization and denitration efficiency levels (operating conditions: discharge power = 19.5 W, gas flow rate = 5 L/min, scrubbing solution = 1% NaOH solution, packing type = D_g 6 mm Dixon ring, packing height = 80 cm).

For the packed scrubber using the NaOH solution, when the liquid/gas ratio reaches 2 L/m³, the desulfurization efficiency reaches more than 99% [33]. In this experiment, the spray density of 1.8 m³/(m²·h) means that the liquid/gas ratio reaches 3 L/m³; therefore, further increases in spray density have little effect on the desulfurization efficiency. The increases in spray density have a greater impact on denitration efficiency, indicating that the demand for gas–liquid mass transfer area for NO_x removal is higher.

On the one hand, increases in spray density will mean the packings will be wetter and the actual gas–liquid mass transfer area will be larger; on the other hand, if the spray density is too high, the liquid film on the packing surface will thicken and flooding will occur, resulting in a sharp pressure drop in the scrubber and a sharp decrease in the gas–liquid mass transfer efficiency [34].

The flooding point is the operating limit of packed scrubber, while the flooding velocity is generally calculated using the Eckert general association diagram [32]. The abscissa can be calculated with the following formula:

$$x = \frac{G_L}{G_V} \left(\frac{\rho_V}{\rho_L} \right)^{0.5}, \quad (6)$$

where G_L is the mass flow rate of scrubbing solution in kg/(m²·s); G_V is the mass flow rate of the gas in kg/(m²·s); ρ_L is the density of the scrubbing solution in kg/m³; ρ_V is the density of the gas in kg/m³.

After the abscissa is calculated, the ordinate y value is obtained according to the flooding point line. The flooding velocity can be calculated according to the following formula:

$$y = \frac{u^2 \psi \phi}{g} \times \frac{\rho_V}{\rho_L} \mu_L^{0.2}, \quad (7)$$

where u is the gas flow rate of the empty tower in m/s; ψ is the ratio of the density of the water to the density of the scrubbing solution; ϕ is the packing factor in 1/m; g is the gravitational acceleration in 9.8 m/s²; μ_L is the viscosity of the scrubbing solution in mPa·s.

The calculation results show that when the spray density increases from 1.8 m³/(m²·h) to 10.8 m³/(m²·h), the flooding velocity decreases from 0.88 m/s to 0.48 m/s. Here, the actual empty tower gas velocity is 0.17 m/s, which is lower than the flooding velocity; therefore, increasing the spray density during the experiment can improve the desulfurization and denitration efficiency levels without causing flooding and reducing the removal efficiency.

3.4. Mass Fraction of NaOH Solution

The effects of the mass fraction of the NaOH solution on desulfurization and denitration efficiency levels are shown in Figure 8. When the mass fraction of the NaOH solution increases from 0% to 1.0%, the desulfurization efficiency increases from 97.2% to 100% and the denitration efficiency increases from 51.0% to 71.8%. With a further increase in the mass fraction of the NaOH solution to 1.5%, the desulfurization efficiency is maintained at 100% and the denitration efficiency slowly increases to 72.6%.

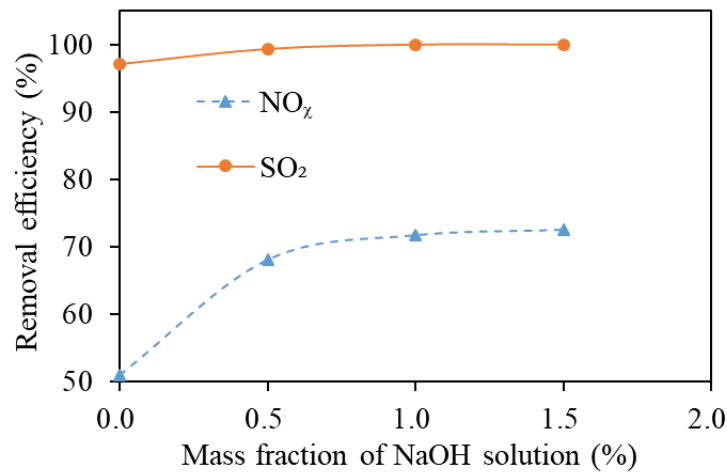


Figure 8. The desulfurization and denitration efficiency levels at various mass fractions of the NaOH solution (operating conditions: discharge power = 19.5 W, the gas flow rate = 5 L/min, spray density = 7.6 m³/(m²·h), packing type = D_g 6 mm Dixon ring, packing height = 80 cm).

In the absorption process of NO_x and SO₂ from the gas phase to the liquid phase, the total mass transfer resistance is the sum of the gas phase mass transfer resistance and liquid phase mass transfer resistance [10,32]:

$$\frac{1}{K_y} = \frac{1}{k_y} + \frac{m}{k_x} \quad (8)$$

where $\frac{1}{K_y}$ is the total mass transfer resistance; $\frac{1}{k_y}$ is the gas phase mass transfer resistance; $\frac{m}{k_x}$ is the liquid phase mass transfer resistance; m is the phase equilibrium constant.

When the absorption capacity of the scrubbing solution is weak, the phase equilibrium constant (m) is large and the liquid phase mass transfer resistance $m/k_x \gg 1/k_y$. Under this condition, the mass transfer resistance is mainly concentrated in the liquid film:

$$\frac{1}{K_y} \approx \frac{m}{k_x} \quad (9)$$

When the scrubbing solution has strong absorption capacity for solutes in the gas phase, m is small and the liquid phase mass transfer resistance $m/k_x \ll 1/k_y$. Under this condition, the mass transfer resistance is mainly concentrated in the liquid phase:

$$\frac{1}{K_y} \approx \frac{1}{k_y} \quad (10)$$

The addition of NaOH in the scrubbing solution makes the desulfurization and denitration process change from physical absorption to chemical absorption. The chemical absorption involves a faster absorption rate. NaOH improves the selectivity and solubility of the scrubbing solution to NO_x and SO₂. With the increase in the NaOH mass fraction in the scrubbing solution, m gradually decreases and the liquid phase mass transfer resistance

m/k_x decreases. When the mass fraction of the NaOH solution exceeds 1.0%, the mass transfer resistance is mainly concentrated in the gas phase; continuing to increase the mass fraction of NaOH solution has little effect on the whole mass transfer process [33].

Table 3 shows the pH values of various mass fractions of NaOH solutions. It can be seen that the pH value of the NaOH solution increases rapidly in the range of 0–1%, which greatly promotes the chemical absorption of NO_x and SO_2 in the liquid phase and reduces the mass transfer resistance in the liquid film. In the range of 1.0–1.5%, the further increase in the NaOH solution mass fraction has little effect on its pH value and the growth of the denitration efficiency slows down significantly.

Table 3. The pH values of various mass fractions of NaOH solutions.

Mass Fraction of NaOH Solution /%	0	0.5	1.0	1.5
pH Value	7.0	13.1	13.4	13.5

3.5. Discharge Power in the DBD Reactor

The discharge power in the DBD reactor has an important influence on the oxidation of NO and SO_2 [30,31]. The desulfurization and denitration efficiency levels of the system at various discharge power levels are presented in Figure 9. The experimental results show that the desulfurization efficiency is always maintained at 99.7–100%, while the denitration efficiency increases significantly from 14% to 94.5% when the discharge power in the DBD reactor increases from 10.9 W to 26.6 W. With further increases in the discharge power, the denitration efficiency increases slowly.

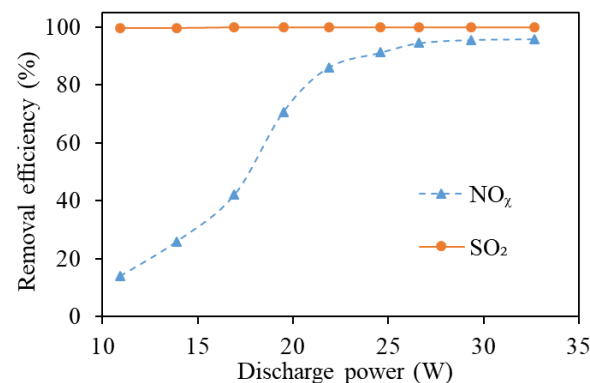


Figure 9. Effects of discharge power on desulfurization and denitration efficiency levels (operating conditions: gas flow rate = 5 L/min, scrubbing solution = 1% NaOH solution, spray density = $7.6 \text{ m}^3/(\text{m}^2 \cdot \text{h})$, packing type = D_g 6 mm Dixon ring, packing height = 80 cm).

SO_2 is very easily absorbed by the alkali solution, while WFGD alone can achieve high desulfurization efficiency; therefore, the discharge power in the DBD reactor has little effect on SO_2 removal. The denitration efficiency is significantly affected by the discharge power, as shown in Figure 9.

Figure 10 shows the effects of the discharge power on NO, NO_2 , and NO_x concentrations and the oxidation degree of NO_x at the outlet of the DBD reactor. With increases in DBD power, the concentrations of NO_x and NO decrease significantly, the concentration of NO_2 increases, and the oxidation degree of NO_x increases gradually. The preoxidation of DBD means most of the is NO directly oxidized to HNO_3 and HNO_2 , then neutralized with the NaOH solution in the scrubber to be removed.

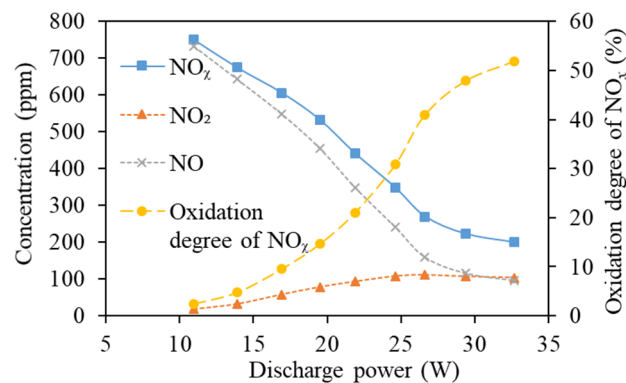
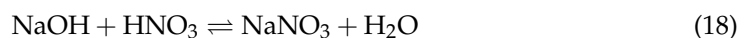
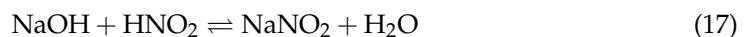
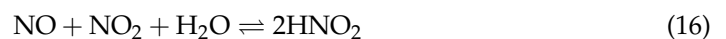
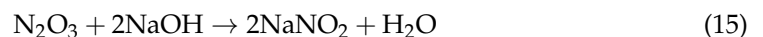
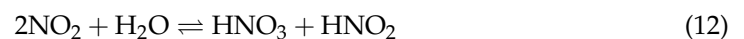


Figure 10. Effects of discharge power on NO, NO₂, and NO_x concentrations and the oxidation degree of NO_x at the outlet of the DBD reactor.

In addition, some of the NO is oxidized to NO₂ by DBD. NO₂ is easily removed by the NaOH solution and can react with NO to generate N₂O₃ and promote the removal of NO, such as in Equations (11)–(18) [12,35]. When the DBD power increases from 10.9 W to 26.6 W, the oxidation degree of NO_x increases rapidly from 2.4% to 41.0% and the removal of NO_x is greatly promoted. Previous research has shown that when the NO_x oxidation degree is 50% under anaerobic conditions, the absorption rate of NO_x in NaOH solution is the highest [34]. Under the oxygen enrichment conditions, the oxidation of NO_x will still occur in the packed scrubber; therefore, when the oxidation degree of NO_x reaches 41%, high denitration efficiency can be achieved and further increases in the NO_x oxidation degree have little impact on the denitration efficiency.



3.6. Simulated Flue Gas Flow Rate

The flue gas flow rate determines the flow velocity and residence time in the scrubbing tower. The effects of the simulated flue gas flow rate on the desulfurization and denitration efficiency levels are shown in Figure 11. In this process, the gas flow rate increases from 3 L/min to 9 L/min, the desulfurization efficiency gradually decreases from 100% to 98.4%, and the denitration efficiency decreases from 82.9% to 53.2%.

Due to the absorbability and low concentration of SO₂, the flue gas flow rate has little effect on the SO₂ removal efficiency during the test. The influence of the flue gas flow rate on the denitration efficiency is more significant. This is mainly for two reasons:

1. The increase in the flue gas flow reduces the gas–liquid mass transfer time of the flue gas in the scrubber, resulting in decreased mass transfer efficiency;
2. The increase in the flue gas flow rate decreases the specific energy density (SED, the energy obtained by unit volume of flue gas), the NO oxidation efficiency in the DBD reactor is reduced, and finally the denitration efficiency is significantly reduced.

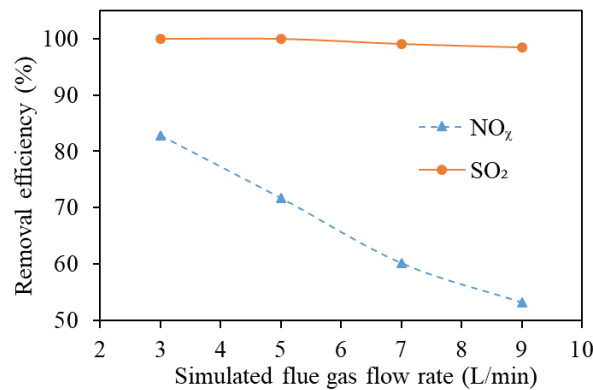


Figure 11. Effects of simulated flue gas flow rate on desulfurization and denitration efficiency levels (operating conditions: discharge power in DBD reactor = 19.5 W, spray density = 7.6 m³/(m²·h), scrubbing solution = 1% NaOH solution, packing type = D_g 6 mm Dixon ring, packing height = 80 cm).

3.7. Weight Analysis of Influencing Factors

From the above single-factor test, it can be seen that various factors have little impact on the desulfurization efficiency of the DBD combined wet scrubbing system, while high desulfurization efficiency is easy to achieve.

The denitration efficiency is the key problem in this system. In order to quantitatively analyze the influence of various factors on the denitration efficiency and to optimize the performance of this system, orthogonal tests were designed to analyze the weights of various factors.

Each factor and its level division are shown in Table 4.

Table 4. The factors and levels involved in the denitration efficiency.

Factor Level	A (-)	B (cm)	C (m ³ /(m ² ·h))	D (%)	E (W)	F (L/min)
1	D _g 10 mm Pall ring	40	1.8	0	10.9	3
2	D _g 6 mm Pall ring	80	5.4	0.5	19.5	5
3	D _g 6 mm Dixon ring	120	10.8	1	26.6	7

A = packing type; B = packing height; C = spray density; D = mass fraction of NaOH solution; E = discharge power in the DBD reactor; F = simulated flue gas flow rate.

An orthogonal table ($L_{18}(3^7)$) was selected to arrange the experiment. The six factors considered in this paper are placed in the first six columns of the table (column 7 is not required). Table 5 shows the specific arrangement and results of the orthogonal test.

Table 5. Arrangement and results of the orthogonal test.

NO.	A	B	C	D	E	F	Results
1	1	1	1	1	1	1	12.17%
2	1	2	2	2	2	2	67.62%
3	1	3	3	3	3	3	81.65%
4	2	1	1	2	2	3	40.68%
5	2	2	2	3	3	1	95.62%
6	2	3	3	1	1	2	15.07%
7	3	1	2	1	3	2	76.02%
8	3	2	3	2	1	3	12.63%
9	3	3	1	3	2	1	79.88%
10	1	1	3	3	2	2	54.85%
11	1	2	1	1	3	3	53.41%
12	1	3	2	2	1	1	17.06%
13	2	1	2	3	1	3	10.94%

Table 5. *Cont.*

NO.	A	B	C	D	E	F	Results
14	2	2	3	1	2	1	65.76%
15	2	3	1	2	3	2	84.95%
16	3	1	3	2	3	1	92.98%
17	3	2	1	3	1	2	16.00%
18	3	3	2	1	2	3	36.56%

The range and variance of each factor in the orthogonal test can reflect its influence on the experimental results. The greater the range and variance, the greater the influence of the factor on the results. Generally, variance is used to evaluate the weights of the factors. The larger the variance of a factor, the greater the weight. The weights of the factors can be calculated using the following formula [36,37]:

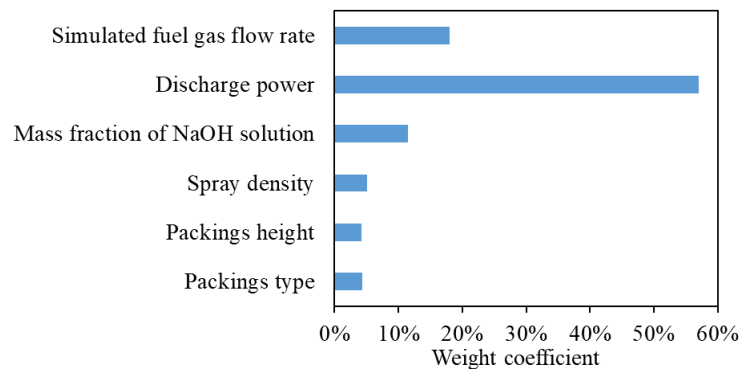
$$S_A = \frac{1}{\alpha} \sum_{i=1}^m K_i^2 - \frac{1}{n} \left(\sum_{k=1}^n x_k \right)^2, \quad (19)$$

$$K_i = \sum_j^{\alpha} x_{ij}, \quad (20)$$

$$w_A = \frac{\sqrt{S_A}}{\sum \sqrt{S_*}}, \quad (21)$$

where S_A is the variance of factor A ; α is the number of tests at each factor level; m represents the levels of factors; n is the total number of tests; K_i is the sum of the i -th level results of the factor; x_k is the test result of number k ; x_{ij} is the result of the i -th level and j -th test of the factor; w_A is the influence weight of factor A ; $\sqrt{S_A}$ is the standard deviation of factor A ; $\sum \sqrt{S_*}$ is the sum of the standard deviations of each factor.

The influence weights of various factors on the denitration efficiency are calculated from the orthogonal test results and are shown in Figure 12.

**Figure 12.** Influence weight of each factor on the denitration efficiency.

The experimental results show that discharge power in the DBD reactor has the greatest impact on the denitration efficiency, the weight coefficient of which is 56.96%. The simulated flue gas flow rate and mass fraction of the NaOH solution also have important effects, the weight coefficients of which are 18.02% and 11.54%, respectively. The spray density, packing type, and packing height have little influence on the denitration efficiency, the weights of which are 5.02%, 4.33%, and 4.16%, respectively.

4. Conclusions

In this paper, an experimental study on desulfurization and denitration was carried out using a DBD reactor combined with a wet scrubber system. The effects of the packing

type, packing height, spray density, mass fraction of the NaOH solution, discharge power in the DBD reactor, and simulated flue gas flow rate on the desulfurization and denitration efficiency levels were analyzed, along with the influence weight of each factor on the denitration efficiency, using orthogonal testing. The main conclusions are as follows:

1. Various factors have little impact on the desulfurization efficiency of the DBD combined wet scrubbing system, while high desulfurization efficiency is easy to achieve. The denitration efficiency is the key problem in this system;
2. The influence weights of the DBD power, simulated flue gas flow rate, mass fraction of the NaOH solution, spray density, packing type, and packing height on denitration efficiency were 56.96%, 18.02%, 11.52%, 5.02%, 4.33%, and 4.16%, respectively.

This paper verifies the feasibility of using DBD combined with a wet scrubbing system for flue gas desulfurization and denitration. The results of this paper will be helpful in optimizing the performance of the system for practical applications in the future.

Author Contributions: Conceptualization, L.Y. and Y.C.; methodology, L.Y. and Y.C.; software, Y.C.; validation, Y.C. and L.Y.; investigation, L.Y. and Y.C.; resources, L.Y. and L.L.; data curation, Y.C.; writing—original draft preparation, L.Y. and Y.C.; writing—review and editing, Y.C., L.L. and L.Y.; visualization, L.Y. and Y.C.; supervision, L.L.; project administration, L.L.; funding acquisition, L.L.. All authors have read and agreed to the published version of the manuscript.

Funding: Please add: This research was funded by National Natural Science Foundation of China (NSFC), grant number 51679176.

Institutional Review Board Statement: Not applicable.

Informed Consent Statement: Not applicable.

Data Availability Statement: Not applicable.

Acknowledgments: The authors are thankful to all personnel who either provided technical support or helped with data collection. We also acknowledge all of the reviewers for their useful comments and suggestions.

Conflicts of Interest: The authors declare no conflict of interest.

References

1. Cengiz, D.; Burak, Z. Environmental and economical assessment of alternative marine fuel. *J. Clean Prod.* **2016**, *113*, 438–449.
2. Ledoux, F.; Roche, C.; Cazier, F.; Beaugard, C.; Courcot, D. Influence of ship emissions on NO_x, SO₂, O₃ and PM concentrations in a North-Sea harbor in France. *J. Environ. Sci.* **2018**, *71*, 56–66. [\[CrossRef\]](#)
3. EGCSA (The Exhaust Gas Cleaning System Association). A Practical Guide to Exhaust Gas Cleaning Systems for the Maritime Industry. 2012. Available online: <http://www.egcsa.com/wp-content/uploads/EGCSA-Handbook-2012-A5-size-.pdf> (accessed on 13 July 2021).
4. Xin, Q.; Hua, Z.S.; Fu, Y.J.; Yang, Y.; Liu, S.J.; Song, H.; Yu, X.N.; Xiao, L.F.; Zheng, C.H.; Gao, X. Investigation on optimal active layer thickness and pore size in dual-layer NH₃-SCR monolith for low SO₂ oxidation by numerical simulation. *Fuel* **2020**, *279*, 118420. [\[CrossRef\]](#)
5. Li, Y.; Xiong, J.; Lin, Y.; Guo, J.; Zhu, T. Distribution of SO₂ oxidation products in the SCR of NO over a V₂O₅/TiO₂ catalyst at different temperatures. *Ind. Eng. Chem. Res.* **2020**, *59*, 5177–5185. [\[CrossRef\]](#)
6. EGCSA (The Exhaust Gas Cleaning System Association). 983 Vessels with Scrubbers or on Order. 2018. Available online: <https://www.egcsa.com/wp-content/uploads/EGCSA-numbers-31-May-2018-7.pdf> (accessed on 13 July 2021).
7. Fang, P.; Chen, X.B.; Tang, Z.J.; Huang, J.H.; Zeng, W.H.; Wu, H.W.; Tang, Z.X.; Cen, C.P. Current research status on air pollutant emission characteristics and control technology of marine diesel engine. *Chem. Ind. Eng. Pro.* **2017**, *36*, 1067–1076.
8. Fang, P.; Cen, C.; Tang, Z.; Zhong, P.; Chen, D.; Chen, Z. Simultaneous removal of SO₂ and NO_x by wet scrubbing using urea solution. *Chem. Eng. J.* **2011**, *168*, 52–59. [\[CrossRef\]](#)
9. Bao, J.; Li, K.; Ning, P.; Wang, C.; Song, X.; Luo, Y.; Sun, X. Study on the role of copper converter slag in simultaneously removing SO₂ and NO_x using KMnO₄/copper converter slag slurry. *J. Environ. Sci.* **2021**, *108*, 33–43. [\[CrossRef\]](#)
10. DESHWAL, B.R.; LEE, H.K. Mass transfer in the absorption of SO₂ and NO_x using aqueous euchlorine scrubbing solution. *J. Environ. Sci.* **2009**, *21*, 155–161. [\[CrossRef\]](#)
11. Yuri, Y.; Hashira, Y.; Daichi, T.; Tomoyuki, K.; Hidekatsu, F.; Masaaki, O. Simultaneous Removal of NO_x and SO_x from Flue Gas of a Glass Melting Furnace using a Combined Ozone Injection and Semi-dry Chemical Process. *Ozone-Sci. Eng.* **2015**, *38*, 211–218.

12. Włodzimierz, K.; Adam, H.; Dariusz, Ł. Influence of Oxidizing Reactor on Flue Gas Denitrification by Ozonation and Possibility of by-Product Separation. *Chem. Process Eng.* **2017**, *38*, 177–191.
13. Si, T.; Wang, C.; Yan, X.N.; Zhang, Y.; Rem, Y.J.; Hu, J.; Edward, J.A. Simultaneous removal of SO₂ and NO_x by a new combined spray-and-scattered-bubble technology based on preozonation: From lab scale to pilot scale. *Appl. Energy* **2019**, *242*, 1528–1538. [[CrossRef](#)]
14. Zou, Y.; Wang, Y.; Liu, X.L.; Zhu, T.Y.; Tian, M.K.; Cai, M.Y. Simultaneous removal of NO_x and SO₂ using two-stage O₃ oxidation combined with Ca(OH)₂ absorption. *Korean J. Chem. Eng.* **2020**, *37*, 1907–1914. [[CrossRef](#)]
15. Ding, J.; Zhong, Q.; Zhang, S.; Song, F.J.; Bu, Y.F. Simultaneous removal of NO_x and SO₂ from coal-fired flue gas by catalytic oxidation-removal process with H₂O₂. *Chem. Eng. J.* **2014**, *243*, 176–182. [[CrossRef](#)]
16. Cui, R.; Ma, S.; Yang, B.; Li, S.; Pei, T.; Li, J.; Wang, J.; Sun, S.; Mi, C. Simultaneous removal of NO_x and SO₂ with H₂O₂ over silica sulfuric acid catalyst synthesized from fly ash. *Waste Manag.* **2020**, *109*, 65–74. [[CrossRef](#)]
17. Han, Z.; Lan, T.; Han, Z.; Yang, S.; Dong, J.; Sun, D.; Yan, Z.; Pan, X.; Song, L. Simultaneous removal of NO and SO₂ from exhaust gas by cyclic scrubbing and online supplementing pH-buffered NaClO₂ solution. *Energ. Fuel* **2019**, *33*, 6591–6599. [[CrossRef](#)]
18. Maria, J.; Dariusz, Ł.; Arkadiusz, Ś.; Mieczysław, A.G.; Mariola, K. Simultaneous removal of NO_x, SO₂, and Hg from flue gas in FGD absorber with oxidant injection (NaClO₂)— full-scale investigation. *J. Air Waste Manage.* **2020**, *70*, 629–640.
19. Yang, S.L.; Pan, X.X.; Han, Z.T.; Zhang, D.S.; Liu, B.J.; Zheng, D.K.; Yan, Z.J. Removal of NO_x and SO₂ from simulated ship emissions using wet scrubbing based on seawater electrolysis technology. *Chem. Eng. J.* **2018**, *331*, 8–15. [[CrossRef](#)]
20. Li, S.; Huang, Y.; Wang, F.; Liu, J.; Feng, F.; Shen, X.; Zheng, Q.; Liu, Z.; Wang, L.; Yan, K. Fundamentals and Environmental Applications of Non-thermal Plasmas: Multi-pollutants Emission Control from Coal-Fired Flue Gas. *Plasma Chem. Plasma Process.* **2014**, *34*, 579–603. [[CrossRef](#)]
21. Ma, S.; Zhao, Y.; Yang, J.; Zhang, S.; Zhang, J.; Zheng, C. Research progress of pollutants removal from coal-fired flue gas using non-thermal plasma. *Renew. Sust. Energ. Rev.* **2017**, *67*, 791–810. [[CrossRef](#)]
22. Chen, R.; Zhang, T.; Wang, J.; Gao, Y.; Wang, J.; Wei, J.; Yu, Q. Recent advances in simultaneous removal of SO₂ and NO_x from exhaust gases: Removal process, mechanism and kinetics. *Chem. Eng. J.* **2020**, *420*, 127588. [[CrossRef](#)]
23. Yu, W.X. Plasma Desulfurization and Denitrification Andits Application in the Study of Marine Diesel Engine Exhaust Treatment. Master's Thesis, Wuhan Textile University, Wuhan, China, 2013.
24. Xie, D.Y.; Sun, Y.; Zhu, T.L.; Ding, L. Removal of NO in mist by the combination of plasma oxidation and chemical absorption. *Energy Fuel* **2016**, *30*, 5071–5076. [[CrossRef](#)]
25. Zhang, C.; Yang, L. One-Dimensional Simulation of Synergistic Desulfurization and Denitrification Processes for Electrostatic Precipitators Based on a Fluid-Chemical Reaction Hybrid Model. *Energies* **2018**, *11*, 3249. [[CrossRef](#)]
26. Chmielewski, A.G.; Zwolińska, E.; Licki, J.; Sun, Y.; Zimek, Z.; Bułka, S. A hybrid plasma-chemical system for high-NO_x flue gas treatment. *Radiat Phys. Chem.* **2017**, *144*, 1–7. [[CrossRef](#)]
27. Gui, S.P.; Zhong, Z.; Liao, Y.J.; Qi, L.; Fu, D. Simultaneous Removal of NO and SO₂ via an Integrated System of Nonthermal Plasma Combined with Catalytic Oxidation and Wet Electrostatic Precipitator. *Energy Fuel* **2019**, *33*, 10078–10089.
28. Zwolińska, E.; Sun, Y.; Chmielewski, A.G.; Pawelec, A.; Bułka, S. Removal of high concentrations of NO_x and SO₂ from diesel off-gases using a hybrid electron beam technology. *Energy Rep.* **2020**, *6*, 952–964. [[CrossRef](#)]
29. Zhao, L.; Sun, Y.X.; Chmielewski, A.G.; Pawelec, A.; Bułka, S. NO Oxidation with NaClO, NaClO₂, and NaClO₃ Solution Using Electron Beam and a One Stage Absorption System. *Plasma Chem. Plasma Process.* **2020**, *40*, 433–447. [[CrossRef](#)]
30. Cai, Y.K.; Lv, L.; Li, P. Study on the effect of structure parameters on NO oxidation in DBD reactor under oxygen-enriched condition. *Appl. Sci.* **2020**, *10*, 6766. [[CrossRef](#)]
31. Cai, Y.K.; Lu, L.; Lu, X.P. The effects of inner electrode diameter on the performance of dielectric barrier discharge reactor for desulfurization and denitrification. *IEEE Trans. Plasma Sci.* **2021**, *49*, 786–793. [[CrossRef](#)]
32. Chen, M.H.; Cong, D.Z.; Fang, T.N.; Qi, M.Z.; Pan, H.L. *Principles of Chemical Engineering (Part II)*, 4th ed.; Chemical Industry Press: Beijing, China, 2015.
33. Liu, D.T. Study on the Absorption, Oxidation Characteristics and Comprehensive Evaluation System of Sodium Alkali Desulfurization of Marine Exhaust Gas. Ph.D. Thesis, Harbin Engineering University, Harbin, China, 2017.
34. Ye, C.W. Study on the Optimum Oxidation Degree of NO in Simultaneous Desulfurization and Denitrification by Urea. Master's Thesis, Wuhan University of Technology, Wuhan, China, 2018.
35. Gao, F.; Liu, F.; Zhang, J.F.; Huang, Y.; Yang, L.C. Mechanism of NO₂ promoting NO absorption by alkali liquor. *Chin. J. Process. Eng.* **2012**, *12*, 796–802.
36. Wu, J.J.; Liu, T.; Zhu, X. Parameter Weight Analysis of Flexible Microgripper Based on Orthogonal Test. *Mach. Tool Hydraul.* **2019**, *48*, 7–11.
37. Chen, K. *Experimental Design and Analysis*, 1st ed.; Tsinghua University Press: Beijing, China, 2005.